Hydrol. Earth Syst. Sci. Discuss., 12, 9337–9391, 2015
www.hydrol-earth-syst-sci-discuss.net/12/9337/2015/
doi:10.5194/hessd-12-9337-2015


Hydrology and Earth System Sciences
Discussions
Open Access



# Evaluation of global fine-resolution precipitation products and their uncertainty quantification in ensemble discharge simulations

**W. Qi[1,2], C. Zhang[1], G. T. Fu[2], C. Sweetapple[2], and H. C. Zhou[1]**

[1]School of Hydraulic Engineering, Dalian University of Technology, Dalian 116024, China
[2]Centre for Water Systems, College of Engineering, Mathematics and Physical Sciences, University of Exeter, North Park Road, Harrison Building, Exeter EX4 4QF, UK

Received: 9 July 2015 – Accepted: 22 August 2015 – Published: 10 September 2015

Correspondence to: C. Zhang (czhang@dlut.edu.cn)

Published by Copernicus Publications on behalf of the European Geosciences Union.

## Abstract

The applicability of six fine-resolution precipitation products, including precipitation radar, infrared, microwave and gauge-based products using different precipitation computation recipes, is comprehensively evaluated using statistical and hydrological methods in a usually-neglected area (northeastern China), and a framework quantifying uncertainty contributions of precipitation products, hydrological models and their interactions to uncertainties in ensemble discharges is proposed. The investigated precipitation products include TRMM3B42, TRMM3B42RT, GLDAS/Noah, APHRODITE, PERSIANN and GSMAP-MVK+. Two hydrological models of different complexities, i.e., a water and energy budget-based distributed hydrological model and a physically-based semi-distributed hydrological model, are employed to investigate the influence of hydrological models on simulated discharges. Results show APHRODITE has high accuracy at a monthly scale compared with other products, and the cloud motion vectors used by GSMAP-MVK+ show huge advantage. These findings could be very useful for validation, refinement and future development of satellite-based products (e.g., NASA Global Precipitation Measurement). Although significant uncertainty exists in heavy precipitation, hydrological models contribute most of the uncertainty in extreme discharges. Interactions between precipitation products and hydrological models contribute significantly to uncertainty in discharge simulations and a better precipitation product does not guarantee a better discharge simulation because of interactions. It is also found that a good discharge simulation depends on a good coalition of a hydrological model and a precipitation product, suggesting that, although the satellite-based precipitation products are not as accurate as the gauge-based product, they could have better performance in discharge simulations when appropriately combined with hydrological models. This information is revealed for the first time and very beneficial for precipitation product applications.





HESSD
12, 9337–9391, 2015

## 1 Introduction

Knowledge of precipitation plays an important role in understanding of the water cycle, and thus in water resources management (Sellers, 1997; Sorooshian et al., 2005; Wang et al., 2005; Ebert et al., 2007; Buarque et al., 2011; Tapiador et al., 2012; Yong et al., 2012; Gao and Liu, 2013; Peng et al., 2014a, b). However, there are little or no precipitation data in many regions throughout the world, particularly in developing countries, mountainous districts and rural areas. For example, Northeast China, which plays an important role in food production to support the country's population and is also an industrial region with many heavy industries, frequently suffers from drought, posing a threat to regional sustainable development. In such areas, due to insufficient gauge observations, alternative precipitation data are required for efficient water resources management.

In recent years, implementation of gauge-based and remote satellite-based precipitation products has become popular, particularly for ungauged catchments (Artan et al., 2007; Jiang et al., 2012; Li et al., 2013; Maggioni et al., 2013; Müller and Thompson, 2013; Xue et al., 2013; Kneis et al., 2014; Meng et al., 2014; Ochoa et al., 2014). Numerous precipitation products have been developed to estimate rainfall, for example:

- Tropical Rainfall Measuring Mission (TRMM) products (Huffman et al., 2007).
- Global Land Data Assimilation System (GLDAS) precipitation products (Kato et al., 2007).
- Ground rain gauge-based interpolation products (APHRODITE) (Xie et al., 2007).
- Precipitation Estimation from Remotely Sensed Information using Artificial Neural Networks (PERSIANN) (Sorooshian et al., 2000, 2002).
- Global Satellite Mapping of Precipitation product (GSMAP) (Kubota et al., 2007; Aonashi et al., 2009).

There are uncertainties in these products. Several studies have been carried out to analyze the uncertainty of TRMM in high latitude regions (Yong et al., 2010, 2012, 2014; Chen et al., 2013a; Zhao and Yatagai, 2014), but studies in northeast China are few. Evaluation of GLDAS data has generally been limited to the United States and other observation-rich regions of the world (Kato et al., 2007); assessments and applications in other regions are rare (Wang et al., 2011; Zhou et al., 2013). The APHRODITE, PERSIANN and GSMAP-MVK+ products are seldom evaluated in northeast China using basin scale gauge data (Zhou et al., 2008). Owing to the high heterogeneity of rainfall across a variety of spatiotemporal scales, the uncertainty characteristics of precipitation products are variable (Asadullah et al., 2008; Dinku et al., 2008; Nikolopoulos et al., 2010; Pan et al., 2010). Thus, in northeast China, it is essential to completely evaluate the applicability of these precipitation products. In addition, it is also worth comparing the performance of different precipitation computation recipes: for example, the artificial neural network function used in PERSIANN, the histogram matching approach used in TRMM3B42, and the cloud motion vectors used in GSMAP-MVK+, because the inter-comparison could reveal the strategies that could be used to obtain more accurate precipitation data.

Many researchers have implemented precipitation products in discharge simulations and reported discharge uncertainties (Hong et al., 2006; Pan et al., 2010; Serpetzoglou et al., 2010). Also, many uncertainty analysis approaches have been introduced to quantify the uncertainty (Beven and Binley, 1992; Freer et al., 1996; Kuczera and Parent, 1998; Beven and Freer, 2001; Peters et al., 2003; Heidari et al., 2006; Blasone et al., 2008). In these prior approaches, one of the popular methods is the generalized likelihood uncertainty estimation (GLUE) technique, introduced by Beven and Binley (1992). This approach outputs probability distributions of model parameters conditioned on observed data, and the uncertainties in model inputs are represented by uncertain parameters. Similar to GLUE, Hong et al. (2006) proposed a Monte Carlo based method to quantify uncertainty in hydrological simulations using satellite precipi-





HESSD
12, 9337–9391, 2015

tation data, in which flow simulation uncertainty is represented by ensemble simulation results.

In addition to uncertainty resulting from the hydrological models, interactions between precipitation products and hydrological models and uncertainty in precipitation data also contribute to uncertainty in simulated discharges. However, to the best of our knowledge, the previous studies have not quantified the respective contributions of precipitation products, hydrological models and their interactions to total discharge simulation uncertainty.

The overall objectives of this paper are: (1) to investigate the applicability of six fine-resolution precipitation products using both statistical and hydrological evaluation methods in the usually-neglected area – northeast China, (2) to propose a framework to quantify the contributions of uncertainties from precipitation products, hydrological models and their interactions to uncertainty in simulated discharges. The precipitation products investigated include TRMM3B42, TRMM3B42RT, GLDAS/Noah (GLDAS_Noah025SUBP_3H), APHRODITE, PERSIANN and GSMAP-MVK+. Two hydrological models with different complexities – a water and energy budget-based distributed hydrological model (WEB-DHM) (Wang et al., 2009a–c) and a physically-based semi-distributed hydrological model TOPMODEL (Beven and Kirkby, 1979) – were employed to investigate the influence of hydrological models on discharge simulations. A series of 8 year data was employed.

The paper is organized as follows. Section 2 introduces the study region, precipitation products, hydrological models and the proposed framework. Section 3 presents the statistical evaluation results. Hydrological evaluations and the implementation of the proposed framework are given in Sect. 4. Summary and conclusions are presented in Sect. 5.





HESSD
12, 9337–9391, 2015

## 2 Materials and methodology

### 2.1 Biliu basin

Biliu basin (2814 km$^2$), located in the coastal region between the China Bohai Sea and the China Huanghai Sea, covers longitudes 122.29 to 122.92° E and latitudes 39.54 to 40.35° N. This basin is characterized by a temperate monsoon marine climate and summer (July to September) is the major rainy season. There are 11 rainfall stations and one discharge gauge which have historical data from January 2000 to December 2007. The major land cover types are forest and farmland and the average annual temperature is 10.6 °C. The average elevation is 240 m. The maximum elevation is 985 m in the northern part which is a mountainous region, and the minimum is 4.5 m in the southern part. The gauge distribution in Biliu is shown in Fig. 1.

### 2.2 Precipitation products

The selected precipitation products are shown in Table 1. These data are all freely available. In these selected precipitation products, APHRODITE is fully based on gauge data; TRMM3B42 and GLDAS are remote satellite estimation with gauge data corrections; while others are remote satellite estimation without gauge data corrections. Remote-based precipitation estimation has many weaknesses, e.g., microwave estimation could miss convective rainfall and typhoon rain because of its sparse time interval resolution; infrared estimation has a higher time interval resolution, but it cannot penetrate thick clouds. Ground rain gauge-based interpolation products are limited by the interpolation algorithm, gauge density and gauge data quality (Xie et al., 2007). Details of data sources used in each precipitation product can be found in Table 1. Detailed introductions of these products are as follows.

TRMM is a joint mission between NASA and Japan Aerospace Exploration Agency designed to monitor and study tropical rainfall (Kummerow et al., 2000; Huffman et al., 2007). Three instruments – a visible infrared radiometer, a TRMM microwave imager





HESSD
12, 9337–9391, 2015

and a precipitation radar – are employed to obtain an accurate precipitation estimation. The TRMM precipitation radar is the first space-based precipitation radar and operates between 35° N and 35° S. Outside this band, the microwave imager is used between 40° N and 40° S, and the visible infrared radiometer data are used between 50° N to 50° S. Usually the precipitation radar is considered to give the most accurate estimation from satellite, and data from it are often used for calibration of passive microwave data from other instruments (Ebert et al., 2007). The post-real-time product used in this study is the TRMM3B42, which utilizes three data sources: the TRMM combined instrument estimation using data from both TRMM precipitation radar and the microwave imager; the GPCP monthly rain gauge analysis developed by the Global Precipitation Climatology Center; and the Climate Assessment and Monitoring System monthly rain gauge analysis. TRMM3B42 applies an infrared to rain rate relationship using histogram matching, while TRMM3B42RT merges microwave and infrared precipitation estimation.

PERSIANN is a product that, using an artificial neural network function, estimates precipitation by combining infrared precipitation estimation and the TRMM combined instrument estimation (which assimilates with TRMM precipitation radar and microwave data). GSMAP-MVK+ uses microwave and infrared precipitation data together and combines cloud motion vectors to generate fine-resolution precipitation estimation.

The Global Land Data Assimilation System (GLDAS) project is an extension of the existing and more mature North American Land Data Assimilation System (Rodell et al., 2004). It integrates satellite- and ground-based data sets for parameterizing, forcing and constraining a few offline land surface models for generating optimal fields of land surface states and fluxes. At present, GLDAS drives four Land Surface Models: Mosaic (Koster and Suarez, 1992), Noah (Chen et al., 1996; Betts et al., 1997; Koren et al., 1999; Ek, 2003), the Community Land Model (Dai et al., 2003) and Variable Infiltration Capacity model (Liang et al., 1994). Among them, the GLDAS/Noah Land Surface Model product (GLDAS_NOAH025SUBP_3H) has a 3 h 0.25° × 0.25°





HESSD
12, 9337–9391, 2015

resolution, which is desirable for basin scale research. The GLDAS precipitation data combine microwave and infrared, and also assimilate gauge observations.

The inter-comparison schemes which mainly include five experiments (Exp 1–Exp 5) are shown in Fig. 2. The five experiments were set up based on the differences among the precipitation products in data types (including data sources and recipes) listed in Table 1: thus the differences in precipitation amounts can reflect the differences in data types. The inter-comparison results could be potentially used to improve products. Exp 1 is to compare TRMM3B42 and TRMM3B42RT. Exp 2 is to compare the differences between TRMM3B42 and PERSIANN. Exp 3 is to compare the most popular satellite product TRMM3B42 and the fully gauge-based product APHRODITE. Exp 4 is to compare TRMM3B42 and GSMAP-MVK+. Exp 5 is to compare GSMAP-MVK+ and GLDAS/Noah.

### 2.3 Criteria for accuracy assessment

Uncertainties of precipitation products are evaluated on the basis of basin-averaged rainfall observations. Four evaluation criteria are used in rainfall amount error assessment: correlation coefficient (CC), root mean square error (RMSE), Nash–Sutcliffe coefficient of efficiency (NSCE) and relative bias (RB). These are calculated as follows:

$$\mathrm{RMSE} = \sqrt{\frac{\sum_{i=1}^{n}(X_{\mathrm{pi}} - X_{\mathrm{oi}})^2}{n}} \quad (1)$$

$$\mathrm{NSCE} = 1 - \frac{\sum_{i=1}^{n}(X_{\mathrm{pi}} - X_{\mathrm{oi}})^2}{\sum_{i=1}^{n}(X_{\mathrm{oi}} - \overline{X_o})^2} \quad (2)$$





HESSD
12, 9337–9391, 2015

Evaluation of global fine-resolution precipitation products

W. Qi et al.

$$\mathrm{RB} = \frac{\sum_{i=1}^{n} X_{\mathrm{pi}} - \sum_{i=1}^{n} X_{\mathrm{oi}}}{\sum_{i=1}^{n} X_{\mathrm{oi}}} \times 100\,\% \tag{3}$$

where $X_{\mathrm{oi}}$ represents observed data; $X_{\mathrm{pi}}$ represents estimated data; $n$ is the total number of data points. A perfect fit should have CC and NSCE values of one. The lower the RMSE and RB, the better the estimation. These comparison criteria have been used by many studies (Ebert et al., 2007; Wang et al., 2011; Yong et al., 2012). In discharge simulation, RMSE and RB are used.

Probability distributions by occurrence and volume are also analyzed, which can provide us with the information on the frequency and on the product error dependence on precipitation intensity (Chen et al., 2013a, b). The critical success index (CSI), probability of detection (POD) and false alarm ratio (FAR) are used to quantify the ability of precipitation products to detect observed rainfall events. These are defined as follows:

$$\mathrm{CSI} = \frac{H}{H+M+F} \tag{4}$$

$$\mathrm{POD} = \frac{H}{H+M} \tag{5}$$

$$\mathrm{FAR} = \frac{F}{H+F} \tag{6}$$

where $H$ is the total number of hits; $M$ is the total number of misses; $F$ is the total number of false alarms (Ebert et al., 2007; Su et al., 2008). A perfect detection should have CSI and POD values equal to one and a FAR value of zero.





HESSD
12, 9337–9391, 2015
Evaluation of global fine-resolution precipitation products
W. Qi et al.

## 2.4 Hydrological models and data

### 2.4.1 WEB-DHM

The distributed biosphere hydrological model, WEB-DHM (Wang et al., 2009a–c), was developed by coupling a simple biosphere scheme (Sellers et al., 1986) with a geomorphology-based hydrological model (Yang, 1998) to describe water, energy and $CO_2$ fluxes at a basin scale. WEB-DHM has been used in several evaluations and applications (Wang et al., 2010a, b; Wang et al., 2012; Shrestha et al., 2013).

WEB-DHM input data include precipitation, temperature, downward solar radiation, long wave radiation, air pressure, wind speed and humidity. With the exception of precipitation, all input data are obtained from automatic weather stations. There are three automatic weather stations near Biliu, and observations from these are obtained from the China Meteorological Data Sharing Service System (downloaded from http://www.cma.gov.cn/2011qxfw/2011qsjgx/). Hourly precipitation data are downscaled from daily rain gauge observations using a stochastic method (Wang et al., 2011). Hourly temperatures are calculated from daily maximum and minimum temperatures using the TEMP model (Parton and Logan, 1981). The estimated temperatures are also further evaluated using daily average temperature. Downward solar radiation is estimated from sunshine duration, temperature and humidity using a hybrid model (Yang et al., 2006). Long wave radiation is obtained from the GLDAS/Noah (Rodell et al., 2004). Air pressure is estimated according to altitude (Yang et al., 2006). These meteorological data are then interpolated to 300 m model cells through inverse-distance weighting. Surface air temperature is further modified with a lapse rate of $6.5\,\mathrm{K\,km^{-1}}$ considering evaluation differences between model cells and meteorological gauges. Gauge rainfall data are also interpolated to 300 m model cells. In addition to the above, the leaf area index and fraction of photosynthetically active radiation data are obtained from level-4 MODIS global products-MOD11A2. Digital Elevation Model (DEM) was from the NASA SRTM (Shuttle Radar Topographic Mission) with a resolution of 30 m × 30 m. We resampled the resolution to 300 m in model calculation to reduce computation cost, while the model processed finer DEM (30 m grid) to generate subgrid parameters (such as hillslope angle and length). The grid slopes vary from 0 to 38°. Land-use data were obtained from the USGS (http://edc2.usgs.gov/glcc/glcc.php). The land-use types have been reclassified to SiB2 land-use types for this study (Sellers et al., 1996). There are six land-use types, with broadleaf and needle leaf trees and short vegetation being the main types. Soil data were obtained from the Food and Agriculture Association (FAO) (2003) Global data product, and there are two types of soil in the basin.

WEB-DHM was calibrated against observed discharges of Biliu. Six main parameters were selected to calibrate using a trial and error approach given consideration of the model computational burden. What we calibrated were parameter multipliers, similar to the study by Wang et al. (2011). The "Trial and error" approach has two steps. First, all the multiplier values are set to 1 which represents the default parameter values from Food and Agriculture Association (FAO) (2003) and SiB2 model. Second, varying the multiplier values until acceptable discharge simulation accuracy is obtained. The calibrated parameter values are listed in Table 2. The simulated daily, monthly and inter-annual results are shown in Fig. 3a, c and e.

### 2.4.2 TOPMODEL

TOPMODEL is a physically-based, variable contributing area model of basin hydrology which attempts to combine the advantages of a simple lumped parameter model with distributed effects (Beven and Kirkby, 1979). Fundamental to TOPMODEL's parameterization are three assumptions: (1) saturated-zone dynamics can be approximated by successive steady-state representations, (2) hydrological gradients of the saturated zone can be approximated by the local topographic surface slope; and (3) the transmissivity profile whose form declines exponentially with increasing vertical depth of the water table or storage is spatially constant. On the basis of above mentioned assumptions, the index of hydrological similarity is represented as the topographic index, $\ln(a/\tan\beta)$, for which $a$ is the area per unit contour length and $\beta$ is the local slope





HESSD
12, 9337–9391, 2015

angle. More detailed descriptions of TOPMODEL and its mathematical formulation can be found in Beven et al. (1979). TOPMODEL has been popularly utilized in many researches across the world (Blazkova and Beven, 1997; Cameron et al., 1999; Hossain and Anagnostou, 2005; Bastola et al., 2008; Gallart et al., 2008; Bouilloud et al., 2010; Qi et al., 2013), because of its relatively simple model structure. The input data of TOPMODEL mainly includes basin averaged precipitation and topographic data which can be estimated from DEM.

Six parameters of TOPMODEL were calibrated using the dynamically dimensioned search algorithm (Tolson and Shoemaker, 2007), and the results are given in Table 3. The ranges were defined based on experience. The simulated daily, monthly and interannual results are shown in Fig. 3b, d and f.

### 2.5 The proposed framework

Figure 4 shows the diagrammatic flowchart of the proposed framework for quantification of uncertainty contributions to ensemble discharges simulated using precipitation products. This framework includes four parts: (a) selection of precipitation products, (b) selection of hydrological models, (c) ensemble discharge simulations using the hydrological models and precipitation products; and (d) quantification of individual and interactive contributions including contributions from precipitation products, hydrological models and interactions between models and products. Because the spatial resolution of selected precipitation products does not correspond with WEB-DHM model cells, the following procedures were carried out in basin average rainfall calculations and discharge simulations: (1) resampling 0.25 or 0.1° precipitation product grids into 300 m × 300 m cells (the grid size used in WEB-DHM simulations), (2) calculating basin average precipitation using 300 m precipitation product grids located within the basin boundary. Diagrammatic descriptions of these procedures are shown in Fig. 1d. Because WEB-DHM needs hourly input data, for the 3 h resolution precipitation products, we assumed rainfall is uniformly distributed within each 3 h period. For daily resolution products, we used the same approach as downscaling observed precipitation data.





HESSD
12, 9337–9391, 2015

This downscaling approach may affect uncertainty in simulated discharge. However, Wang et al. (2011) have already successfully applied the downscaling approach, and showing that the influence is negligible.

The total ensemble uncertainty $Y$ is the variance of discharges. To relate $Y$ to the uncertainty sources, the superscripts $j$ and $k$ in $Y^{j,k}$ represent a combination of precipitation product $j$ and hydrological model $k$

$$Y^{j,k} = P^j + M^k + PM^{j,k} \tag{7}$$

where $P$ represents the effect of $j$th precipitation product, $M$ represents the effect of $k$th hydrological model, and $PM$ represents the interaction effect. In this study, $j$ varies from one to six, and $k$ varies from one to two. Details of the quantification are explained in the follow sections. The chain in which precipitation products and hydrological models are combined is shown in Fig. 5.

### 2.5.1 Subsampling approach

It is argued that the ANOVA approach is based on a biased variance estimator that underestimates variance when the sample size is small (Bosshard et al., 2013). To reduce the effect of the biased estimator on quantification of variance contributions, Bosshard et al. (2013) proposed a subsampling method, which was used in this paper. In the subsampling method, the superscript $j$ in Eq. (7) is replaced with $\mathbf{g}(h,i)$. According to Bosshard et al. (2013), in each subsampling iteration $i$, data from two products should be selected out of all the six products, and thus 15 combinations can be obtained. Therefore, the superscript $\mathbf{g}$ becomes a $2 \times 15$ matrix:

$$\mathbf{g} = \begin{pmatrix} 1 & 1 & \dots & 1 & 2 & 2 & \dots & 4 & 4 & 5 \\ 2 & 3 & \dots & 6 & 3 & 4 & \dots & 5 & 6 & 6 \end{pmatrix} \tag{8}$$





HESSD
12, 9337–9391, 2015

### 2.5.2 Uncertainty contribution decomposition

Based on the ANOVA theory (Bosshard et al., 2013), total error variance (SST) can be divided into sums of squares due to the individual effects as:

$$\mathrm{SST} = \mathrm{SSA} + \mathrm{SSB} + \mathrm{SSI} \tag{9}$$

where SSA is the error contribution of precipitation products, SSB is the error contribution of hydrological models and SSI is the error contribution of their interactions.

The terms can be estimated using the subsampling procedure as follows:

$$\mathrm{SST}_i = \sum_{h=1}^{H}\sum_{k=1}^{K}\left(Y^{\mathbf{g}(h,i),k} - Y^{\mathbf{g}(o,i),o}\right)^2 \tag{10}$$

$$\mathrm{SSA}_i = K \cdot \sum_{h=1}^{H}\left(Y^{\mathbf{g}(h,i),o} - Y^{\mathbf{g}(o,i),o}\right)^2 \tag{11}$$

$$\mathrm{SSB}_i = H \cdot \sum_{k=1}^{K}\left(Y^{\mathbf{g}(o,i),k} - Y^{\mathbf{g}(o,i),o}\right)^2 \tag{12}$$

$$\mathrm{SSI}_i = \sum_{h=1}^{H}\sum_{k=1}^{K}\left(Y^{\mathbf{g}(h,i),k} - Y^{\mathbf{g}(h,i),o} - Y^{\mathbf{g}(o,i),k} + Y^{\mathbf{g}(o,i),o}\right)^2 \tag{13}$$

where symbol $^{\circ}$ indicates averaging over the particular index; $H$ is the number of precipitation products (six in this study) and $K$ is the number of hydrological models (two in this study). Then the variation fraction $\eta^2$ is calculated as follows:

$$\eta^2_{\mathrm{precipitation}} = \frac{1}{I}\sum_{i=1}^{I}\frac{\mathrm{SSA}_i}{\mathrm{SST}_i} \tag{14}$$

$$\eta^2_{\mathrm{model}} = \frac{1}{I}\sum_{i=1}^{I}\frac{\mathrm{SSB}_i}{\mathrm{SST}_i} \tag{15}$$





HESSD
12, 9337–9391, 2015
Evaluation of global fine-resolution precipitation products
W. Qi et al.

$$\eta^2_{\text{interaction}} = \frac{1}{I}\sum_{i=1}^{I}\frac{\text{SSI}_i}{\text{SST}_i} \quad (16)$$

$\eta^2$ has a value between 0 and 1, which represent 0 and 100 % contribution to the overall uncertainty of simulated discharges respectively. $I$ equals 15 in this study. As shown in Eqs. 14–16, the subsampling approach is necessary because it guarantees that every contributor has the same denominator $I$. This same denominator makes sure that the inter-comparison among precipitation contribution, model contribution and interaction contribution is free of influence from the sampling number of precipitation products and hydrological models.

# 3 Statistical evaluations

## 3.1 Daily and monthly scales

Comparison of precipitation product data and observations at a daily scale is shown in Fig. 6. Observations are shown on the $x$ axis and precipitation product data are shown on the $y$ axis. Four criteria, RMSE, CC, NSCE and RB, are also shown. Most of the selected precipitation products are 0.25° resolutions except GSMAP-MVK+. For 0.25° precipitation products, there are 11 grids locating inside our study basin, and there are 11 in situ rainfall gauges in study basin also. The number is the same, and therefore we used basin average rainfall amount in our evaluations. GSMAP-MVK+ is the best product and PERSIANN is the worst with respect to RMSE and NSCE. GSMAP-MVK+ is also the best with respect to CC, while GLDAS is the worst with a CC value of 0.55. With respect to RB, APHRODITE performs best and GSMAP-MVK+ the second best, while TRMM3B42RT the worst with an RB value of −38 %. None of the products can outperform others in terms of all the statistical criteria, which may be due to the different limitations of satellite sensors and inverse algorithms used to produce the products. This situation shows that the selection of the best precipitation products is difficult.





HESSD
12, 9337–9391, 2015

TRMM3B42RT and TRMM3B42 underestimate precipitation amounts. This underestimation may be because convective rainfall always happens in summer in northeast China, and indicates the limitation of TRMM algorithms in high latitude regions with convective rainfall. This type of rainfall has a large rainfall amount within a short time period and, therefore, cannot be captured by microwave imager. This type of rainfall may also have a thick cloud that is impenetrable by infrared (Ebert et al., 2007). Thus microwave and infrared estimation could underestimate rainfall. Compared with TRMM3B42RT, TRMM3B42 provides an improvement in RB. This improvement may be attributed to the assimilation with precipitation radar, gauge data and histogram matching. Compared with APHRODITE and GSMAP-MVK+, TRMM3B42 has low accuracy as represented by RB. This implies that the retrieval algorithm used by TRMM3B42 still needs to be improved with respect to RB. The reason why APHRODITE outperforms TRMM3B42 is that APHRODITE is a gauge-based product. GSMAP-MVK+ outperforms TRMM3B42 in terms of RB may be due to the cloud motion vectors it uses. This information suggests that TRMM3B42 could be improved with respect to RB by the use of cloud motion vectors or APHRODITE. In addition, the artificial neural network function used by PERSIANN could help to improve RB, because only PERSIANN overestimates rainfall amount among all the products. In terms of RMSE, NSCE and CC, TRMM3B42 may be improved using the cloud motion vectors, since GSMAP-MVK+ provides the lowest RMSE and highest CC and NSCE of all the analyzed products. Compared with GSMAP-MVK+, GLDAS/Noah precipitation shows low accuracy in all the criteria, which indicates the gauge correction method in GLDAS/Noah is not as effective as the cloud motion vectors in GSMAP-MVK+, even though they use similar data sources: IR and MW.

Comparison of precipitation product data and observations at a monthly scale is shown in Fig. 7. Observations are shown on the $x$ axis and precipitation product data are shown on the $y$ axis. RMSE, CC, NSCE and RB, are also shown. Here, the APHRODITE product (Fig. 7d) performs best based on RMSE, CC, NSCE and RB. GLDAS/Noah is the worst in terms of RMSE and NSCE. With respect to CC,





HESSD
12, 9337–9391, 2015

GLDAS and TRMM3B42 are equal worst, with CC values of 0.81. The results also show that PERSIANN overestimates precipitation amount, while Li et al. (2013) found PERSIANN to underestimate rainfall in south China. This may attribute to the different latitudes of the study regions, suggesting that the accuracy of PERSIANN is related to latitude. PERSIANN data are adjusted using the TRMM microwave imager, and Yong et al. (2010) found that the error structures of TRMM microwave imager are closely associated with latitudes: thus the precision of PERSIANN data is influenced by geographical locations. In addition, this information also implies that the artificial neural network function of PERSIANN may be incapable of reducing the geographical dependence of TRMM microwave imager error.

Figure 8 shows time series of average monthly precipitation data against gauge observations during the period 2000–2007. Each curve represents a different precipitation product. GLDAS data (Fig. 8a) seriously underestimate high rainfall. Similarly, GSMAP-MVK+, TRMM3B42 and TRMM3B42RT all underestimate peak precipitation intensity but TRMM3B42 is a little better. These products all use microwave or infrared precipitation estimation, and this confirms the weakness of microwave and infrared estimation in the case of heavy precipitation (Asadullah et al., 2008; Dinku et al., 2008). PERSIANN overestimates heavy precipitation significantly, which may be a result of the artificial neural network function used. Comparatively, APHRODITE has a medium performance. Thus, if TRMM3B42 wants to improve heavy precipitation estimation, the artificial neural network function and APHRODITE products could be helpful.

### 3.2 Inter-annual evaluations

Figure 9 shows the inter-annual average monthly precipitation. Each curve represents a different product data. PERSIANN overestimates in all the 12 months, while others underestimate, especially during the summer. This may result from the artificial neural network function and limitations of infrared and microwave estimation. APHRODITE data are relatively close to observations. Compared with TRMM3B42RT, TRMM3B42 is better, which indicates the precipitation radar, gauge corrections and histogram match-





HESSD
12, 9337–9391, 2015

ing used by TRMM3B42 impact positively on accuracy. During the summer (July and August), discrepancies between products become larger, implying that uncertainties in rainfall estimates from different products increase. With a decrease of rainfall magnitude, the discrepancies between products reduce, indicating that uncertainties in rainfall estimates decrease. This information implies that the differences in precipitation estimation algorithms are related to precipitation magnitudes: the larger the rainfall magnitudes, the greater the differences.

### 3.3 Probability distribution evaluations

Figure 10 shows cumulative probability distribution functions (CDF) by occurrence (CDFc) and by volume (CDFv) for precipitation products. Probabilities are shown on the *y* axis, and the *x* axis shows rainfall intensity with a 1 mm day$^{-1}$ interval log space.

PERSIANN is the best by both occurrence and volume. However, for CDFc, TRMM3B42RT is the worst, and, for CDFv, TRMM3B42RT and GLDAS/Noah are comparable and worse than others. All precipitation products overestimate probabilities by occurrence and by volume except larger rainfall intensity. This may be because the precipitation products underestimate rain intensity except that PERSIANN overestimates high rain intensity (recall the results in Sect. 3.1). The results differ from those of Li et al. (2013), in which PERSIANN performs the worst. This results from differences in latitudes (in the study of Li et al. (2013), south China was studied). This difference confirms the finding in Sect. 3.1 that the artificial neural network function of PERSIANN may be incapable of reducing the geographical dependence of TRMM microwave imager error, and the precision of PERSIANN is influenced by geographical locations.

### 3.4 Contingency statistics

Figure 11 shows the probability of detection, false alarm ratio and critical success index for each precipitation product.





HESSD
12, 9337–9391, 2015

PERSIANN has the highest false alarm ratio among the products, while TRMM3B42RT has the lowest. The false alarm ratio of TRMM3B42 is larger than TRMM3B42RT, which indicates that the precipitation radar, gauge corrections and histogram matching used by TRMM3B42 do not provide positive effects on false alarm ratio and may give rise to uncertainty in false alarm ratio. To improve the false alarm ratio of TRMM3B42, using the artificial neural network function would be ineffective; GSMAP-MVK+ has a lower false alarm ratio than TRMM3B42, indicating that use of cloud motion vectors could potentially improve TRMM3B42 with respect to the false alarm ratio.

No trends are observed for the false alarm ratio, which means the false alarm ratio dependence on rainfall magnitude is weak. This implies that microwave precipitation estimation, infrared precipitation estimation and the inversing algorithm used by APHRODITE may have weak dependence on rainfall magnitude in terms of the false alarm ratio. However, Chen et al. (2013a) found the false alarm ratios of TRMM3B42 and TRMM3B42RT to increase with an increase in rainfall intensity. The differences are attributed mainly to observed data. In the study of Chen et al. (2013a), national rain gauge data were employed, whereas in this study more detailed basin data are used.

Among all selected products, GLDAS/Noah has the lowest probability of detection and critical success index during periods of high rainfall intensity, while APHRODITE retains a high probability of detection and critical success index. This is because APHRODITE uses gauge observations, and implies that the APHRODITE algorithm is effective. PERSIANN has comparable probability of detection with APHRODITE, which indicates that the artificial neural network function used by PERSIANN would be a good tool for probability of detection. The critical success index of GSMAP-MVK+ is also comparable with APHRODITE, suggesting that the cloud motion vectors used by GSMAP-MVK+ would be useful for improving the critical success index. Compared with TRMM3B42RT, TRMM3B42 has greater probability of detection and comparable critical success index. This information implies that retrieval algorithm of TRMM3B42





HESSD
12, 9337–9391, 2015

provides positive effects on probability of detection, but not significant positive impacts on critical success index.

Decreasing trends are observed for all products in terms of probability of detection and critical success index, matching the results of Chen et al. (2013a) for TRMM3B42 and TRMM3B42RT. This indicates that probability of detection and critical success index have relatively strong dependence on rainfall magnitude, and implies microwave and infrared precipitation estimation may have relatively strong dependence on rainfall magnitude in terms of probability of detection and critical success index.

## 4 Hydrological evaluations

### 4.1 Daily scale discharges

Figures 12 and 13 display scatterplots of discharges during the period 2000–2007 simulated using WEB-DHM and TOPMODEL against observations at a daily scale. Two criteria, NSCE and RB, are shown.

In the case of WEB-DHM simulations, the best NSCE (0.41) corresponds with APHORODITE (Fig. 12d), while the best value for RB (1 %) corresponds with GLDAS/Noah. In the case of TOMODEL simulations, the best NSCE (0.41) corresponds with APHORODITE, and the best value for RB (−24 %) corresponds with APHORODITE also. Although the best NSCE is the same for both WEB-DHM and TOPMODEL simulations and corresponding product is also the same, there is a large difference in the best RB values. Big differences exist in large discharges as well, and TOPMODEL underestimates almost all larger discharges except in a simulation using PERSIANN. At the daily scale precipitation amount evaluation, the worst RB is −38 %, corresponding with TRMM3B42RT (Fig. 6c). However, in WEB-DHM discharge simulation, the worst RB (218 %) corresponds with PERSIANN, and, in TOPMODEL simulation, the worst RB (−62 %) corresponds with TRMM3B42RT. These differences stem





HESSD
12, 9337–9391, 2015

from differences in hydrological models and interactions between hydrological models and precipitation product data.

All RB criteria at the daily scale precipitation evaluations (recall the results in Fig. 6) are nonlinearly amplified by TOPMODEL, while in the case of WBE-DHM, some are amplified and the others are decreased. These differences result from the influence of hydrological models and interactions between precipitation products and hydrological models. These results reveal that a hydrological model can amplify uncertainties in input data but also reduce uncertainties, and that the propagation of uncertainties from precipitation data to discharge simulations is nonlinear, which may be due to the nonlinear runoff generation process in hydrological models. This finding is consistent with the research by Yong et al. (2010).

## 4.2 Monthly scale discharges

Figures 14 and 15 display scatterplots of discharges during the period 2000–2007 simulated using WEB-DHM and TOPMODEL against observations at a monthly scale. Two criteria, NSCE and RB, are shown.

In the case of WEB-DHM, the best NSCE and RB values are 0.73 and 1 %, which corresponding with TRMM3B42 and GLDAS respectively. In the case of TOPMODEL, they are 0.58 and −24 %, corresponding with PERSIANN and APHRODITE respectively. In the case of the WEB-DHM simulation using PERSIANN data, almost all peak discharges are overestimated, but in the case of TOPMODEL simulations, many peak discharges are underestimated using PERSIANN data. These differences are mainly because of hydrological model influence and interactive influence between precipitation data and models.

The combination of WEB-DHM and TRMM3B42 shows a great performance, with NSCE and RB values of up to 0.73 and −7 %, even though TRMM3B42 is not the best in monthly scale precipitation data evaluation. This is a comprehensive result influenced by both hydrological models and precipitation data, and implies that accurate discharge simulation does not solely depend on the accuracy of a precipitation product.

At the monthly scale, although APHRODITE is the best precipitation product and WEB-DHM model has better performance than TOPMODEL in calibration (Fig. 3c and d), the combination of APHRODITE and WEB-DHM is not better in the discharge simulation, which can be shown by comparing Fig. 14d with Fig. 15d. This is due to the interactive influence between hydrological models and precipitation products, and implies that the interactions between models and products could be significant and have a big influence on discharge simulations. In addition, comparison of Fig. 14d and b shows that discharge simulation of APHRODITE is worse than TRMM3B42, even though APHRODITE is the best precipitation product in terms of all the selected criteria at a monthly scale precipitation amount evaluation. This information shows that better precipitation products do not guarantee better discharge simulations. This is counter intuitive because the influence of interactions between precipitation products and hydrological models is usually ignored: thus our result provides improved understanding about discharge simulations using precipitation products. These results imply that, although the satellite-based precipitation products are not as accurate as gauge-based products in rainfall amount estimation, they could have a better performance in discharge simulations if the combination of precipitation product and hydrological model is good.

Even though WEB-DHM has a better performance than TOPMODEL in calibration (Fig. 3c and d), discharge simulation results may not be better than TOPMODEL (for example, the results shown in Fig. 15f are better than those in Fig. 14f). This implies that complex and advanced models could lose their advantages if the input data and models were not good coalitions, and models which perform worse in calibration could lead to better discharge simulations due to the interactive influence between models and precipitation products.

### 4.3 Inter-annual average monthly discharges

Figure 16 shows inter-annual average monthly discharges of all selected precipitation products during the period 2000–2007. In the case of TOPMODEL, PERSIANN





HESSD
12, 9337–9391, 2015

agrees well with observations, and all products underestimate discharges in August. In the case of WEB-DHM, GLDAS data and TRMM3B42 data have a better performance than other data but, with the exception of PERSIANN, all products underestimate peak discharge in August. The simulation results show huge differences even though Fig. 3e and f show TOPMDOEL and WEB-DHM have almost the same performance using observed data; this is because of the impacts of interactive influence between hydrological models and precipitation products. This shows that similar hydrological model performance and the same precipitation product do not imply similar discharge simulation accuracy.

## 4.4 Uncertainty source quantification

All above results suggest that discharge simulations are influenced by precipitation products, hydrological models and interactions between hydrological models and precipitation products. Thus it is essential to quantify the respective influence. Figure 17a and b shows contributions of precipitation products, hydrological models and their interactions to uncertainties in monthly average discharges and different flow quantiles respectively. Figure 17b shows quantiles computed at a daily time step. The contributions of uncertainty sources are represented by stripes.

Figure 17a shows that precipitation data contribute most of the uncertainty in discharges, and is more significant than hydrological models. Interactions between hydrological models and precipitation products have significant contributions, at a similar level to those from hydrological models. In summer (July to September), the contribution of precipitation data is less than most other months except March. However, the uncertainty in precipitation intensity increases in summer (recall the results in Sect. 3.2). In non-summer months except March, the uncertainty contribution from precipitation products is larger than in summer. These differences maybe result from the nonlinear propagation of uncertainty through hydrological models. In March, the contribution of hydrological models is larger than in other months, which may result from the decrease





HESSD
12, 9337–9391, 2015

in influences of interactions and precipitation products, and from the nonlinear influence of the hydrological models.

Figure 17b shows that, for small and large discharges, hydrological models contribute most of the uncertainties. For middle magnitude flows, precipitation products contribute the majority, and the contribution of interactions is significant and of similar magnitude to the contribution from hydrological models. The contribution of interactions is larger for middle magnitude flows than for small and large discharges. This may result from an increase in interaction, implying that interaction effects are influenced by discharge magnitude. The different contributions of interactions for various magnitude flows may be because different magnitude rainfall data could trigger different hydrological processes (Herman et al., 2013). Small discharges mainly come from groundwater flow which is relatively stable and does not need much rainfall to be triggered, and large flow is mainly controlled by overland flow when heavy precipitation occurs. Middle magnitude flow, on the other hand, consists of contributions from groundwater flows, lateral subsurface flows and overland flows. It is more complex and can be triggered by various magnitude rainfalls – thus interactions are more changeable.

Although heavy rainfall data have high uncertainty (recall the results in Sect. 3.1), precipitation products don't contribute the most uncertainty in large discharges (Fig. 17b). This may be because the nonlinear propagation of uncertainty through hydrological models enlarges the influence of hydrological models, and implies that high uncertainties in extreme rainfall do not mean high uncertainties in extreme discharges. This information suggests that for better implementation of precipitation products, precipitation products may need to provide some information on combinations with hydrological models and on the suitability of the combinations for different magnitude flows.

In this study, because hydrological model parameters were calibrated using gauge observations, the hydrological model parameter uncertainty was not considered. Although the uncertainty contribution results in this study may not be transferable to other basins, the proposed framework provides a useful tool for quantifying uncertainty contributions in discharge simulations using precipitation products.





HESSD
12, 9337–9391, 2015

## 5 Summary and conclusions

This research comprehensively assesses the applicability of six precipitation products with fine spatial and temporal resolutions at a high latitude region in northeast China. This area is usually-neglected in precipitation data accuracy assessments. Both statistical and hydrological evaluation methods at multi-temporal scales were used in the assessment. A framework is proposed to quantify uncertainty contributions of precipitation products, hydrological models and their interactions to simulated discharges. These products include TRMM version 7 products (TRMM3B42 and TRMM3B42RT), GLDAS, APHRODITE, PERSIANN and GSMAP-MVK+. The fully distributed WEB-DHM and semi-distributed TOPMODEL were employed to investigate the influence of hydrological models on simulated discharges. The results show the uncertainty characteristics of the six products, and reveal strategies that could improve precipitation products. This information could be able to provide references for future precipitation product development. The proposed framework can reveal hydrological simulation uncertainties using precipitation products: thus provides useful information on precipitation product applications. The following conclusions are presented on the basis of this study.

First, at daily scale, selecting the best precipitation products is very difficult, while, at a monthly scale, APHRODITE has the best performance in terms of NSCE, RB, RMSE, and CC, and also retains a high probability of detection and critical success index. This information implies that the APHRODITE algorithm is effective, and APHRODITE could be a very good data set to refine and validate satellite-based precipitation products.

Second, the cloud motion vectors used by GSMAP-MVK+ show huge advantage, and could be used to improve TRMM3B42 in RB, NSCE, RMSE, CC, false alarm ratio and critical success index, while the artificial neural network function used by PERSIANN could be useful for improvements of probability of detection, precipitation probability distribution estimation and heavy rainfall estimation. At present, the new precipitation estimation mission – NASA Global Precipitation Measurement (GPM) –





HESSD
12, 9337–9391, 2015

combines the artificial neural network function of PERSIANN and precipitation radar-matching of TRMM Multi-satellite Precipitation Analysis. However, this finding implies that incorporating cloud motion vectors into GPM could be better.

Third, it is found that, although high uncertainty exists in heavy rainfall, hydrological models contribute mostly to the uncertainty in extreme discharges. This may result from the nonlinear propagation of uncertainty through hydrological models enlarges the influence of hydrological models, and implies that high uncertainties in extreme rainfall do not mean high uncertainties in extreme discharges.

Fourth, interactions between hydrological models and precipitation products contribute significantly to uncertainty in discharge simulations, and interactive impacts are influenced by discharge magnitude. Because of interactive effects, for hydrological models with similar performances in calibration, using the same precipitation products for discharge simulations does not provide a similar level of accuracy in discharge simulations, and in fact significantly different predictions could be obtained. In addition, this finding implies that only considering precipitation products or hydrological model uncertainties could result in overestimation of precipitation product contribution and hydrological model contribution to discharge uncertainty.

Fifth, a good discharge simulation depends on a good coalition of a hydrological model and a precipitation product, and a better precipitation product does not guarantee a better discharge simulation, whereas it is possible that a hydrological model which is worse in calibration may generate a better discharge simulation. This information suggests that, although the satellite-based precipitation products are not as accurate as the gauge-based product, they could have better performance in discharge simulations when appropriately combined with hydrological models.

In the future, calculating deterministic discharge simulations considering precipitation product uncertainties and hydrological model uncertainties together should be studied because above results show product uncertainties and model uncertainties all are important. In addition, recalibrating hydrological models using precipitation products may reduce the interactive influence between hydrological models and precipi-





HESSD
12, 9337–9391, 2015

tation products on simulated discharges, and this may explain why recalibration can improve discharge simulation accuracy. This should be verified in future work. Further, future work is encouraged to develop good collations with hydrological models, as a good collation could help to achieve the same aim as improving the accuracy of precipitation products: precisely simulating discharges. Future research is also encouraged to incorporate cloud motion vectors into GPM because of the good performance of cloud motion vectors.

*Acknowledgements.* This study was supported by the National Basic Research Programme (973 programme) of China (Grant No. 2013CB036400). The first author gratefully acknowledges the financial support provided by the China Scholarship Council. The APHRODITE data were downloaded from http://www.chikyu.ac.jp/precip/products/index.html. The TRMM3B42 data are downloaded from http://mirador.gsfc.nasa.gov/cgi-bin/mirador/presentNavigation.pl?tree=project&project=TRMM&dataGroup=Gridded. TRMM3B42RT data are downloaded from ftp://trmmopen.nascom.nasa.gov/pub/merged/mergeIRMicro/. PERSIANN data are downloaded from http://chrs.web.uci.edu/persiann/data.html. GSMAP-MVK+ data are downloaded from http://sharaku.eorc.jaxa.jp/GSMaP_crest/. The GLDAS data are downloaded from http://mirador.gsfc.nasa.gov/cgi-bin/mirador/homepageAlt.pl?keyword=GLDAS_NOAH025SUBP_3H. The data of Biliu basin were obtained from the Biliu reservoir administration.

## References

Aonashi, K., Awaka, J., Hirose, M., Kozu, T., Kubota, T., Liu, G., Shige, S., Kida, S., Seto, S., Takahashi, N., and Takayabu, Y. N.: GSMaP passive microwave precipitation retrieval algorithm: algorithm description and validation, J. Meteorol. Soc. Jpn., 87A, 119–136, 2009.

Artan, G., Gadain, H., Smith, J. L., Asante, K., Bandaragoda, C. J., and Verdin, J. P.: Adequacy of satellite derived rainfall data for stream flow modeling, Nat. Hazards, 43, 167–185, 2007.

Asadullah, A., McIntyre, N., and Kigobe, M. A. X.: Evaluation of five satellite products for estimation of rainfall over Uganda, Hydrolog. Sci. J., 53, 1137–1150, 2008.

Bastola, S., Ishidaira, H., and Takeuchi, K.: Regionalisation of hydrological model parameters under parameter uncertainty: a case study involving TOPMODEL and basins across the globe, J. Hydrol., 357, 188–206, 2008.

Betts, A. K., Chen, F., Mitchell, K. E., and Janjic, Z. I.: Assessment of the land surface and boundary layer models in two operational versions of the NCEP Eta Model using FIFE data, Mon. Weather Rev., 125, 2896–2916, 1997.

Beven, K. J. and Binley, A.: the future of distributed models: model calibration and uncertainty prediction, Hydrol. Process., 6, 279–98, 1992.

Beven, K. J. and Freer, J. E.: Equifinality, data assimilation, and uncertainty estimation in mechanistic modelling of complex environmental systems using the GLUE methodology, J. Hydrol., 249, 11–29, 2001.

Beven, K. J. and Kirkby, M. J.: A physically based, variable contributing area model of basin hydrology, Hydrological Sciences Bulletin, 24, 43–69, 1979.

Blasone, R.-S., Vrugt, J. A., Madsen, H., Rosbjerg, D., Robinson, B. A., and Zyvoloski, G. A.: Generalized likelihood uncertainty estimation (GLUE) using adaptive Markov Chain Monte Carlo sampling, Adv. Water Resour., 31, 630–648, 2008.

Blazkova, S. and Beven, K.: Flood frequency prediction for data limited catchments in the Czech Republic using a stochastic rainfall model and TOPMODEL, J. Hydrol., 195, 256–278, 1997.

Bosshard, T., Carambia, M., Goergen, K., Kotlarski, S., Krahe, P., Zappa, M., and Schär, C.: Quantifying uncertainty sources in an ensemble of hydrological climate-impact projections, Water Resour. Res., 49, 1523–1536, 2013.

Bouilloud, L., Chancibault, K., Vincendon, B., Ducrocq, V., Habets, F., Saulnier, G.-M., Anquetin, S., Martin, E., and Noilhan, J.: Coupling the ISBA Land Surface Model and the TOPMODEL Hydrological Model for mediterranean flash-flood forecasting: description, calibration, and validation, J. Hydrometeorol., 11, 315–333, 2010.

Buarque, D. C., de Paiva, R. C. D., Clarke, R. T., and Mendes, C. A. B.: A comparison of Amazon rainfall characteristics derived from TRMM, CMORPH and the Brazilian national rain gauge network, J. Geophys. Res., 116, D19105, doi:10.1029/2011JD016060, 2011.

Cameron, D. S., Beven, K. J., Tawn, J., Blazkova, S., and Naden, P.: Flood frequency estimation by continuous simulation for a gauged upland catchment (with uncertainty), J. Hydrol., 219, 169–187, 1999.






HESSD
12, 9337–9391, 2015

Chen, F., Mitchell, K., Schaake, J., Xue, Y., Pan, H.-L., Koren, V., Duan, Q. Y., Ek, M., and Betts, A.: Modeling of land surface evaporation by four schemes and comparison with FIFE observations, J. Geophys. Res., 101, 7251–7268, 1996.

Chen, S., Hong, Y., Cao, Q., Gourley, J. J., Kirstetter, P.-E., Yong, B., Tian, Y., Zhang, Z., Shen, Y., Hu, J., and Hardy, J.: Similarity and difference of the two successive V6 and V7 TRMM multisatellite precipitation analysis performance over China, J. Geophys. Res.-Atmos., 118, 13060–13074, 2013a.

Chen, S., Hong, Y., Gourley, J. J., Huffman, G. J., Tian, Y., Cao, Q., Yong, B., Kirstetter, P.-E., Hu, J., Hardy, J., Li, Z., Khan, S. I., and Xue, X.: Evaluation of the successive V6 and V7 TRMM multisatellite precipitation analysis over the continental United States, Water Resour. Res., 49, 8174–8186, 2013b.

Dai, Y., Zeng, X., Dickinson, R. E., Baker, I., Bonan, G. B., Bosilovich, M. G., Denning, A. S., Dirmeyer, P. A., Houser, P. R., Niu, G., Oleson, K. W., Schlosser, C. A., and Yang, Z.-L.: The common land model, B. Am. Meteorol. Soc., 84, 1013–1023, 2003.

Dinku, T., Connor, S. J., Ceccato, P., and Ropelewski, C. F.: Comparison of global gridded precipitation products over a mountainous region of Africa, Int. J. Climatol., 28, 1627–1638, 2008.

Ebert, E. E., Janowiak, J. E., and Kidd, C.: Comparison of near-real-time precipitation estimates from satellite observations and numerical models, B. Am. Meteorol. Soc., 88, 47–64, 2007.

Ek, M. B.: Implementation of Noah land surface model advances in the National Centers for Environmental Prediction operational mesoscale Eta model, J. Geophys. Res., 108, 8851, doi:10.1029/2002JD003296, 2003.

Food and Agriculture Association (FAO): Digital soil map of the world and derived soil properties, land and water digital media series [CD-ROM], Rome, Italy, 2003.

Freer, J. E., Beven, K. J., and Ambroise, B.: Bayesian estimation of uncertainty in runoff prediction and the value of data: an application of the GLUE approach, Water Resour. Res., 32, 2161–2173, 1996.

Gallart, F., Latron, J., Llorens, P., and Beven, K. J.: Upscaling discrete internal observations for obtaining catchment-averaged TOPMODEL parameters in a small Mediterranean mountain basin, Phys. Chem. Earth, 33, 1090–1094, 2008.

Gao, Y. C. and Liu, M. F.: Evaluation of high-resolution satellite precipitation products using rain gauge observations over the Tibetan Plateau, Hydrol. Earth Syst. Sci., 17, 837–849, doi:10.5194/hess-17-837-2013, 2013.

Heidari, A., Saghafian, B., and Maknoon, R.: Assessment of flood forecasting lead time based on generalized likelihood uncertainty estimation approach, Stoch. Env. Res. Risk A., 20, 363–380, 2006.

Herman, J. D., Reed, P. M., and Wagener, T.: Time-varying sensitivity analysis clarifies the effects of watershed model formulation on model behavior, Water Resour. Res., 49, 1400–1414, 2013.

Hong, Y., Hsu, K.-l., Moradkhani, H., and Sorooshian, S.: Uncertainty quantification of satellite precipitation estimation and Monte Carlo assessment of the error propagation into hydrologic response, Water Resour. Res., 42, W08421, doi:10.1029/2005WR004398, 2006.

Hossain, F. and Anagnostou, E. N.: Assessment of a stochastic interpolation based parameter sampling scheme for efficient uncertainty analyses of hydrologic models, Comput. Geosci., 31, 497–512, 2005.

Huffman, G. J., Bolvin, D. T., Nelkin, E. J., Wolff, D. B., Adler, R. F., Gu, G., Hong, Y., Bowman, K. P., and Stocker, E. F.: The TRMM Multisatellite Precipitation Analysis (TMPA): quasi-global, multiyear, combined-sensor precipitation estimates at fine scales, J. Hydrometeorol., 8, 38–55, 2007.

Jiang, S., Ren, L., Hong, Y., Yong, B., Yang, X., Yuan, F., and Ma, M.: Comprehensive evaluation of multi-satellite precipitation products with a dense rain gauge network and optimally merging their simulated hydrological flows using the Bayesian model averaging method, J. Hydrol., 452–453, 213–225, 2012.

Kato, H., Rodell, M., Beyrich, F., Cleugh, H., Gorsel, E.v., Liu, H., and Meyers, T. P.: Sensitivity of land surface simulations to model physics, land characteristics, and forcings, at four CEOP sites, J. Meteorol. Soc. Jpn., 85A, 187–204, 2007.

Kneis, D., Chatterjee, C., and Singh, R.: Evaluation of TRMM rainfall estimates over a large Indian river basin (Mahanadi), Hydrol. Earth Syst. Sci., 18, 2493–2502, doi:10.5194/hess-18-2493-2014, 2014.

Koren, V., Schaake, J., Mitchell, K., Duan, Q. Y., Chen, F., and Baker, J. M.: A parameterization of snowpack and frozen ground intended for NCEP weather and climate models, J. Geophys. Res., 104, 19569–19585, 1999.

Koster, R. D. and Suarez, M. J.: Modeling the land surface boundary in climate models as a composite of independent vegetation stands, J. Geophys. Res.-Atmos., 97, 2697–2715, 1992.

Kubota, T., Shige, S., Hashizurne, H., Aonashi, K., Takahashi, N., Seto, S., Hirose, M., Takayabu, Y. N., Ushio, T., Nakagawa, K., Wanami, K., Kachi, M., and Okamoto, K.: Global precipitation map using satellite-borne microwave radiometers by the GSMaP project: production and validation, IEEE T. Geosci. Remote, 45, 2259–2275, 2007.

Kuczera, G. and Parent, E.: Monte Carlo assessment of parameter uncertainty in conceptual catchment models – the Metropolis algorithm, J. Hydrol., 211, 69–85, 1998.

Kummerow, C., Simpson, J., and Thiele, O.: The status of the Tropical Rainfall Measuring Mission (TRMM) after two years in orbit, J. Appl. Meteorol. Clim., 39, 1965–1982, 2000.

Li, Z., Yang, D., and Hong, Y.: Multi-scale evaluation of high-resolution multi-sensor blended global precipitation products over the Yangtze River, J. Hydrol., 500, 157–169, 2013.

Liang, X., Lettenmaier, D. P., Wood, E. F., and Burges, S. J.: A simple hydrologically based model of land-surface water and energy fluxes for general-circulation models, J. Geophys. Res.-Atmos., 99, 14415–14428, 1994.

Maggioni, V., Vergara, H. J., Anagnostou, E. N., Gourley, J. J., Hong, Y., and Stampoulis, D.: Investigating the applicability of error correction ensembles of satellite rainfall products in river flow simulations, J. Hydrometeorol., 14, 1194–1211, 2013.

Meng, J., Li, L., Hao, Z., Wang, J., and Shao, Q.: Suitability of TRMM satellite rainfall in driving a distributed hydrological model in the source region of Yellow River, J. Hydrol., 509, 320–332, 2014.

Müller, M. F. and Thompson, S. E.: Bias adjustment of satellite rainfall data through stochastic modeling: methods development and application to Nepal, Adv. Water Resour., 60, 121–134, 2013.

Nikolopoulos, E. I., Anagnostou, E. N., Hossain, F., Gebremichael, M., and Borga, M.: Understanding the scale relationships of uncertainty propagation of satellite rainfall through a distributed hydrologic model, J. Hydrometeorol., 11, 520–532, 2010.

Ochoa, A., Pineda, L., Crespo, P., and Willems, P.: Evaluation of TRMM 3B42 precipitation estimates and WRF retrospective precipitation simulation over the Pacific–Andean region of Ecuador and Peru, Hydrol. Earth Syst. Sci., 18, 3179–3193, doi:10.5194/hess-18-3179-2014, 2014.

Pan, M., Li, H., and Wood, E.: Assessing the skill of satellite-based precipitation estimates in hydrologic applications, Water Resour. Res., 46, W09535, doi:10.1029/2009WR008290, 2010.





HESSD

12, 9337–9391, 2015

Parton, W. J. and Logan, J. A.: A model for diurnal variation in soil and air temperature, Agr. Meteorol., 23, 205–216, 1981.
Peng, Z., Wang, Q. J., Bennett, J. C., Pokhrel, P., and Wang, Z.: Seasonal precipitation forecasts over China using monthly large-scale oceanic-atmospheric indices, J. Hydrol., 519, 792–802, 2014a.
Peng, Z., Wang, Q. J., Bennett, J. C., Schepen, A., Pappenberger, F., Pokhrel, P., and Wang, Z.: Statistical calibration and bridging of ECMWF System4 outputs for forecasting seasonal precipitation over China, J. Geophys. Res.-Atmos., 119, 7116–7135, 2014b.
Peters, N. E., Freer, J., and Beven, K.: Modelling hydrologic responses in a small forested catchment (Panola Mountain, Georgia, USA): a comparison of the original and a new dynamic TOPMODEL, Hydrol. Process., 17, 345–362, 2003.
Qi, W., Zhang, C., Chu, J., and Zhou, H.: Sobols sensitivity analysis for TOPMODEL hydrological model: a case study for the Biliu River Basin, China, Journal of Hydrology and Environment Research, 1, 1–10, 2013.
Rodell, M., Houser, P. R., Jambor, U., Gottschalck, J., Mitchell, K., Meng, C. J., Arsenault, K., Cosgrove, B., Radakovich, J., Bosilovich, M., Entin, J. K., Walker, J. P., Lohmann, D., and Toll, D.: The Global Land Data Assimilation System, B. Am. Meteorol. Soc., 85, 381–394, 2004.
Sellers, P. J.: Modeling the exchanges of energy, water, and carbon between continents and the atmosphere, Science, 275, 502–509, 1997.
Sellers, P. J., Mintz, Y., Sud, Y. C., and Dalcher, A.: A Simple Biosphere Model (SIB) for use within general circulation models, J. Atmos. Sci., 43, 505–531, 1986.
Sellers, P. J., Randall, D. A., Collatz, G. J., Berry, J. A., Field, C. B., Dazlich, D. A., Zhang, C., Collelo, G. D., and Bounoua, L.: A revised land surface parameterization (SiB2) for atmospheric GCMS. Part I: Model formulation, J. Climate, 9, 676–705, 1996.
Serpetzoglou, E., Anagnostou, E. N., Papadopoulos, A., Nikolopoulos, E. I., and Maggioni, V.: Error propagation of remote sensing rainfall estimates in soil moisture prediction from a land surface model, J. Hydrometeorol., 11, 705–720, 2010.
Shrestha, M., Wang, L., Koike, T., Tsutsui, H., Xue, Y., and Hirabayashi, Y.: Correcting basin-scale snowfall in a mountainous basin using a distributed snowmelt model and remote-sensing data, Hydrol. Earth Syst. Sci., 18, 747–761, doi:10.5194/hess-18-747-2014, 2014.

Sorooshian, S., Hsu, K. L., Gao, X., Gupta, H. V., Imam, B., and Braithwaite, D.: Evaluation of PERSIANN system satellite-based estimates of tropical rainfall, B. Am. Meteorol. Soc., 81, 2035–2046, 2000.

Sorooshian, S., Gao, X., Hsu, K., Maddox, R. A., Hong, Y., Gupta, H. V., and Imam, B.: Diurnal variability of tropical rainfall retrieved from combined GOES and TRMM satellite information, J. Climate, 15, 983–1001, 2002.

Sorooshian, S., Lawford, R. G., Try, P., Rossow, W., Roads, J., Polcher, J., Sommeria, G., and Schifer, R.: Water and energy cycles: investigating the links, WMO Bull., 54, 58–64, 2005.

Su, F., Hong, Y., and Lettenmaier, D. P.: Evaluation of TRMM Multisatellite Precipitation Analysis (TMPA) and its utility in hydrologic prediction in the La Plata basin, J. Hydrometeorol., 9, 622–640, 2008.

Tapiador, F. J., Turk, F. J., Petersen, W., Hou, A. Y., García-Ortega, E., Machado, L. A. T., Angelis, C. F., Salio, P., Kidd, C., Huffman, G. J., and de Castro, M.: Global precipitation measurement: methods, datasets and applications, Atmos. Res., 104–105, 70–97, 2012.

Tolson, B. A. and Shoemaker, C. A.: Dynamically dimensioned search algorithm for computationally efficient watershed model calibration, Water Resour. Res., 43, W01413, doi:10.1029/2005WR004723, 2007.

Wang, D., Wang, G., and Anagnostou, E. N.: Use of satellite-based precipitation observation in improving the parameterization of canopy hydrological processes in land surface models, J. Hydrometeorol., 6, 745–763, 2005.

Wang, F., Wang, L., Koike, T., Zhou, H., Yang, K., Wang, A., and Li, W.: Evaluation and application of a fine-resolution global data set in a semiarid mesoscale river basin with a distributed biosphere hydrological model, J. Geophys. Res., 116, D21108, doi:10.1029/2011JD015990, 2011.

Wang, F., Wang, L., Zhou, H., Saavedra Valeriano, O. C., Koike, T., and Li, W.: Ensemble hydrological prediction-based real-time optimization of a multiobjective reservoir during flood season in a semiarid basin with global numerical weather predictions, Water Resour. Res., 48, W07520, doi:10.1029/2011WR011366, 2012.

Wang, L., Koike, T., Yang, D. W., and Yang, K.: Improving the hydrology of the Simple Biosphere Model 2 and its evaluation within the framework of a distributed hydrological model, Hydrolog. Sci. J., 54, 989–1006, 2009a.

Wang, L., Koike, T., Yang, K., Jackson, T. J., Bindlish, R., and Yang, D.: Development of a distributed biosphere hydrological model and its evaluation with the Southern Great Plains Experiments (SGP97 and SGP99), J. Geophys. Res., 114, D08107, doi:10.1029/2008JD010800, 2009b.

Wang, L., Koike, T., Yang, K., and Yeh, P. J.-F.: Assessment of a distributed biosphere hydrological model against streamflow and MODIS land surface temperature in the upper Tone River Basin, J. Hydrol., 377, 21–34, 2009c.

Wang, L., Koike, T., Yang, K., Jin, R., and Li, H.: Frozen soil parameterization in a distributed biosphere hydrological model, Hydrol. Earth Syst. Sci., 14, 557–571, doi:10.5194/hess-14-557-2010, 2010a.

Wang, L., Wang, Z., Koike, T., Yin, H., Yang, D., and He, S.: The assessment of surface water resources for the semi-arid Yongding River Basin from 1956 to 2000 and the impact of land use change, Hydrol. Process., 24, 1123–1132, 2010b.

Xie, P., Chen, M., Yang, S., Yatagai, A., Hayasaka, T., Fukushima, Y., and Liu, C.: A gauge-based analysis of daily precipitation over East Asia, J. Hydrometeorol., 8, 607–626, 2007.

Xue, X., Hong, Y., Limaye, A. S., Gourley, J. J., Huffman, G. J., Khan, S. I., Dorji, C., and Chen, S.: Statistical and hydrological evaluation of TRMM-based multi-satellite precipitation analysis over the Wangchu basin of Bhutan: are the latest satellite precipitation products 3B42V7 ready for use in ungauged basins?, J. Hydrol., 499, 91–99, 2013.

Yang, D.: Distributed Hydrological Model Using Hillslope Discretization Based on Catchment Area Function: Development and Applications, University of Tokyo, Tokyo, 1998.

Yang, K., Koike, T., and Ye, B.: Improving estimation of hourly, daily, and monthly solar radiation by importing global data sets, Agr. Forest Meteorol., 137, 43–55, 2006.

Yong, B., Ren, L.-L., Hong, Y., Wang, J.-H., Gourley, J. J., Jiang, S.-H., Chen, X., and Wang, W.: Hydrologic evaluation of multisatellite precipitation analysis standard precipitation products in basins beyond its inclined latitude band: a case study in Laohahe basin, China, Water Resour. Res., 46, W07542, doi:10.1029/2009WR008965, 2010.

Yong, B., Hong, Y., Ren, L.-L., Gourley, J. J., Huffman, G. J., Chen, X., Wang, W., and Khan, S. I.: Assessment of evolving TRMM-based multisatellite real-time precipitation estimation methods and their impacts on hydrologic prediction in a high latitude basin, J. Geophys. Res., 117, D09108, doi:10.1029/2011JD017069, 2012.

Yong, B., Chen, B., Gourley, J. J., Ren, L., Hong, Y., Chen, X., Wang, W., Chen, S., and Gong, L.: Intercomparison of the Version-6 and Version-7 TMPA precipitation products over high and low latitudes basins with independent gauge networks: is the newer version better in both

real-time and post-real-time analysis for water resources and hydrologic extremes?, J. Hydrol., 508, 77–87, 2014.
Zhao, T. and Yatagai, A.: Evaluation of TRMM 3B42 product using a new gauge-based analysis of daily precipitation over China, Int. J. Climatol., 34, 2749–2762, 2014.
Zhou, T., Yu, R., Chen, H., Dai, A., and Pan, Y.: Summer precipitation frequency, intensity, and diurnal cycle over China: a comparison of satellite data with rain gauge observations, J. Climate, 21, 3997–4010, 2008.
Zhou, X. Y., Zhang, Y. Q., Yang, Y. H., Yang, Y. M., and Han, S. M.: Evaluation of anomalies in GLDAS-1996 dataset, Water Sci. Technol., 67, 1718–1727, 2013.





HESSD
12, 9337–9391, 2015

**Table 1.** Precipitation products.

| Product | Spatial resolution | Temporal resolution | Areal coverage | Start date | Type |
|---|---|---|---|---|---|
| TRMM3B42 | 0.25° | 3 h | Global 50° N–S | 1 Jan 1998 | PR + IR + MW + gauge + HM |
| TRMM3B42RT | 0.25° | 3 h | Global 50° N–S | 1 Mar 2000 | IR + MW |
| GLDAS/Noah | 0.25° | 3 h | Global 90° N–60° S | 24 Feb 2000 | IR + MW + gauge |
| GSMAP-MVK+ | 0.1° | 1 h | Global 60° N–S | 1 Mar 2000 | IR + MW + CMV |
| PERSIANN | 0.25° | 3 h | Global 60° N–S | 1 Mar 2000 | PR + IR + MW + ANN |
| APHRODITE | 0.25° | 1 day | 60–150° E, 15° S–55° N | 1961 to 2007 | gauge |

PR: precipitation radar; IR: infrared estimation; MW: microwave estimation; HM: histogram matching; CMV: cloud motion vectors; ANN: artificial neural network.





HESSD
12, 9337–9391, 2015

**Table 2.** WEB-DHM parameters.

| Symbol (units) | Brief description | Basin-averaged value |
|---|---|---|
| KS ($mm\,h^{-1}$) | Saturated hydraulic conductivity for soil surface | 26.43 |
| Anik | Hydraulic conductivity anisotropy ratio | 11.49 |
| Sstmax (mm) | Maximum surface water storage | 42.75 |
| Kg ($mm\,h^{-1}$) | Hydraulic conductivity for groundwater | 0.36 |
| alpha | van Genuchten parameter | 0.01 |
| *n* | van Genuchten parameter | 1.88 |





HESSD
12, 9337–9391, 2015

**Table 3.** TOPMODEL parameters.

| Name (units) | Description | Lower bound | Upper bound | Calibration |
|---|---|---|---|---|
| SZM (m) | form of the exponential decline in conductivity | 0.01 | 0.04 | 0.019 |
| LNT0 ($m^2 h^{-1}$) | effective lateral saturated transmissivity | −25 | 1 | −11.911 |
| RV ($m^2 h^{-1}$) | hill slope routing velocity | 2000 | 5000 | 2608.4 |
| $SR_{max}$ (m) | maximum root zone storage | 0.001 | 0.01 | 0.006 |
| $SR_0$ (m) | initial root zone deficit | 0 | 0.01 | 0.005 |
| TD ($m h^{-1}$) | unsaturated zone time delay per unit deficit | 2 | 4 | 2.885 |



HESSD
12, 9337–9391, 2015

Evaluation of global fine-resolution precipitation products

W. Qi et al.

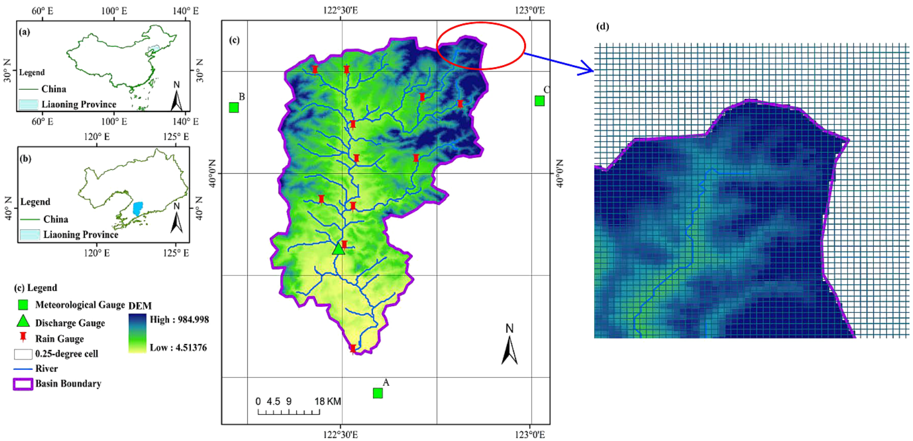


**Figure 1.** Biliu basin: **(a)** the location of Liaoning province within China; **(b)** the location of Biliu basin within Liaoning province; **(c)** the distributions of rain gauges, discharge gauge, automatic weather stations, digital elevation model, and diagrammatic 0.25° precipitation cells; and **(d)** diagrammatic description of downscaling the 0.25° precipitation cells to 300 m × 300 m cells, and retrieving the 300 m × 300 m cells located within the basin boundary.



HESSD
12, 9337–9391, 2015

Evaluation of global fine-resolution precipitation products

W. Qi et al.

Title Page
Abstract | Introduction
Conclusions | References
Tables | Figures
◂◂ | ▸▸
◂ | ▸
Back | Close
Full Screen / Esc
Printer-friendly Version
Interactive Discussion

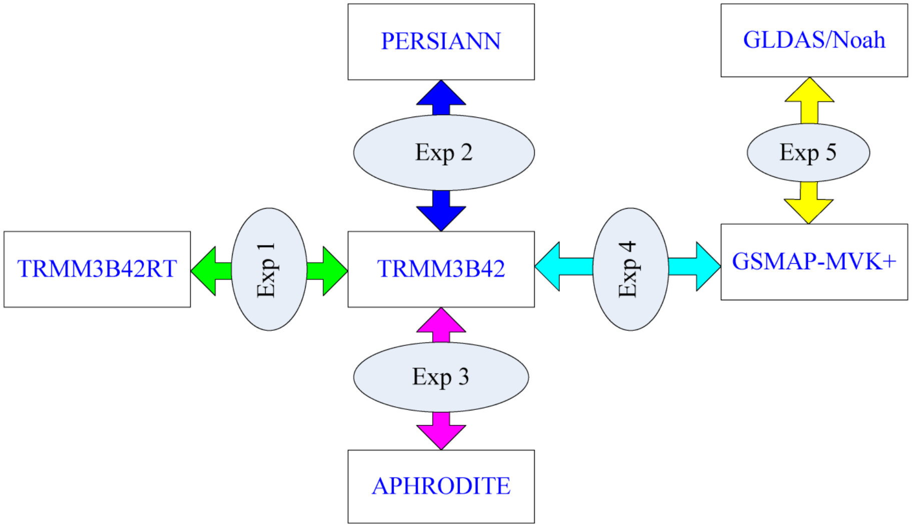


**Figure 2.** Inter-comparison schemes which mainly include five experiments (Exp 1–Exp 5). These experiments were set up based on the differences among the precipitation products in data types (including data sources and recipes). Exp 1 is to compare TRMM3B42 and TRMM3B42RT. Exp 2 is to compare the differences between TRMM3B42 and PERSIANN. Exp 3 is to compare the most popular satellite product TRMM3B42 and the fully gauge-based product APHRODITE. Exp 4 is to compare TRMM3B42 and GSMAP-MVK+. Exp 5 is to compare GSMAP-MVK+ and GLDAS/Noah.





HESSD
12, 9337–9391, 2015

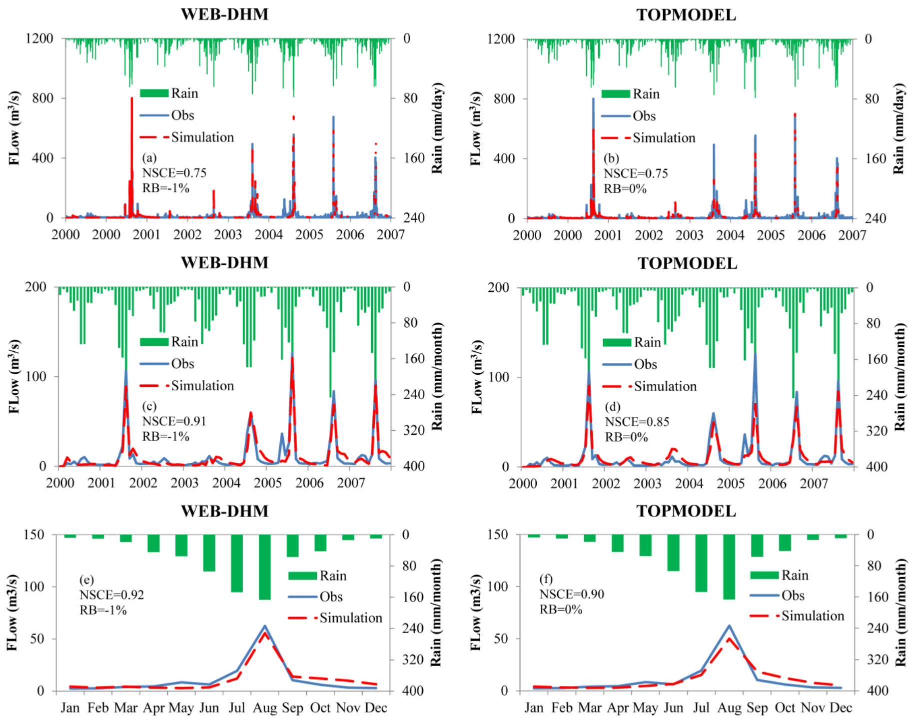


**Figure 3.** Observed and simulated flow using WEB-DHM and TOPMODEL from 2000 to 2007.

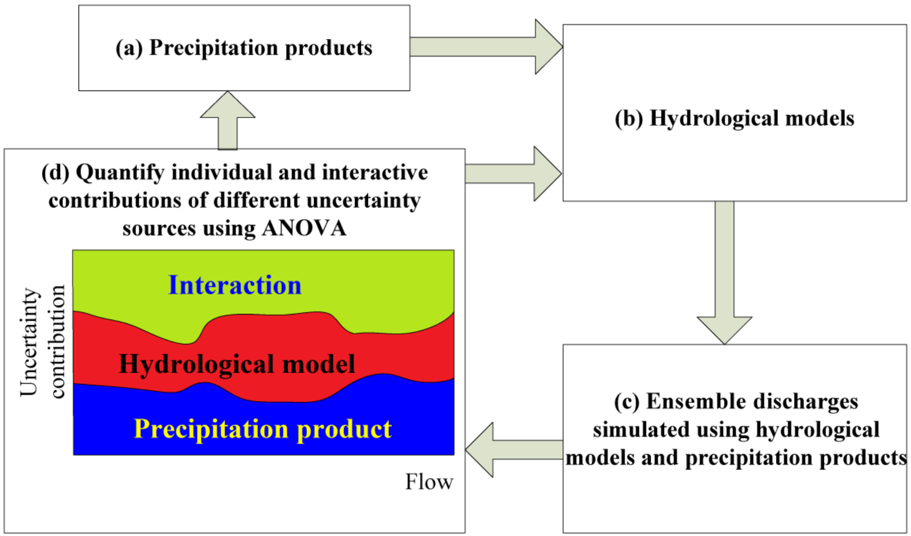


**Figure 4.** Diagrammatic flowchart of the proposed framework for quantification of uncertainty contributions to ensemble discharges simulated using precipitation products.

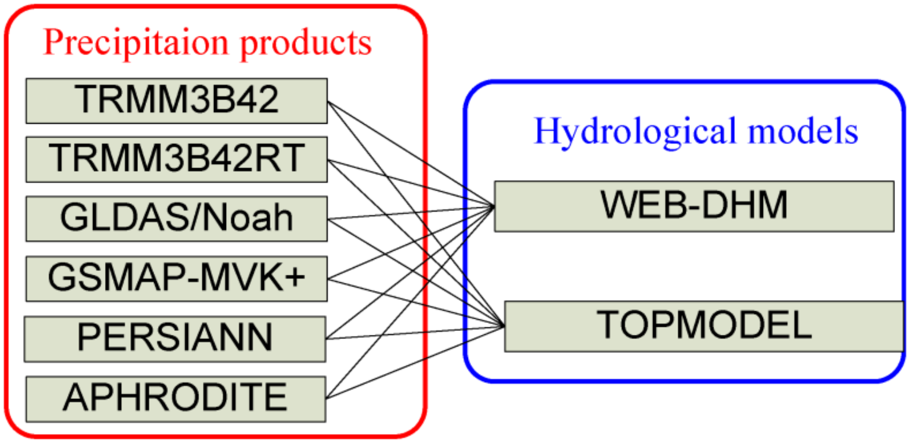


**Figure 5.** Combinations of precipitation products and hydrological models.





HESSD
12, 9337–9391, 2015

Evaluation of global fine-resolution precipitation products

W. Qi et al.

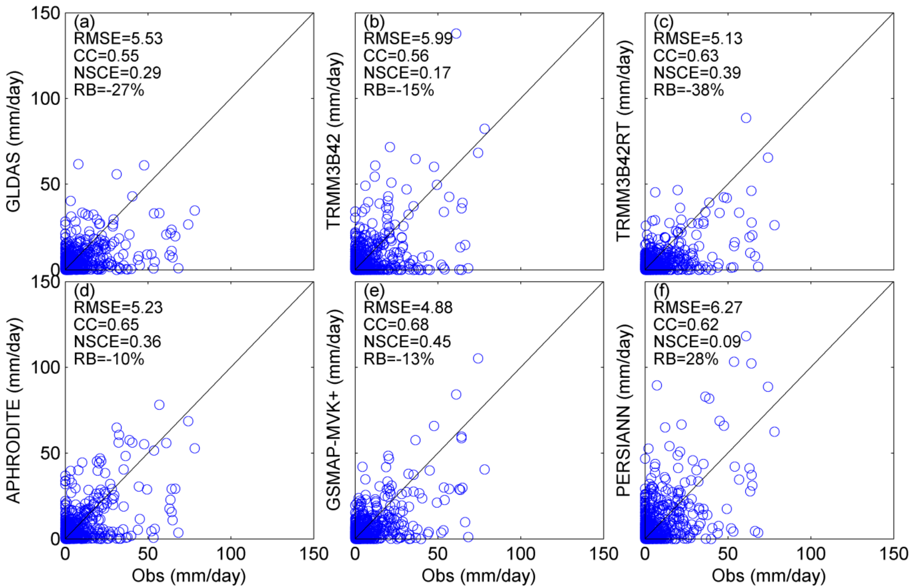


**Figure 6.** Scatterplots of precipitation products vs. gauge observations at a daily scale.





HESSD
12, 9337–9391, 2015

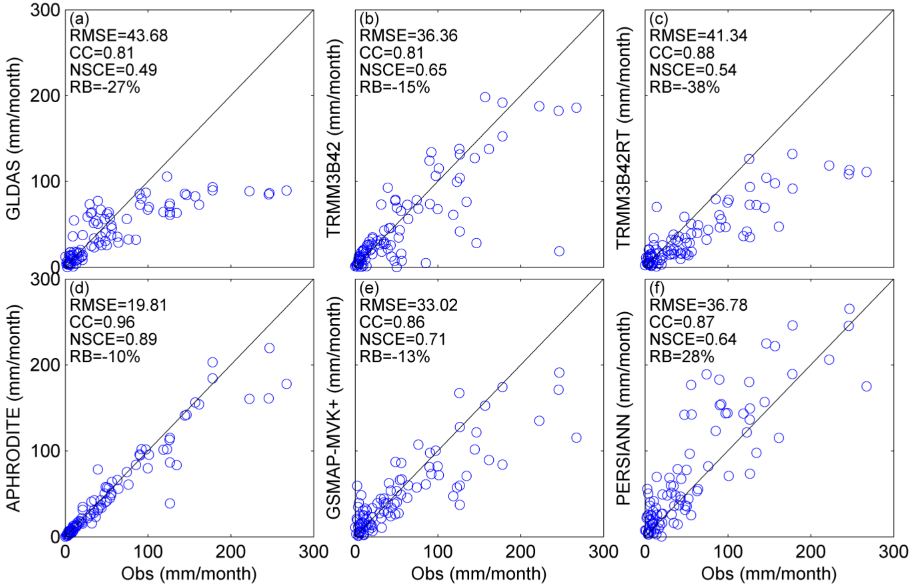


**Figure 7.** Scatterplots of precipitation products vs. gauge observations at a monthly scale.





HESSD
12, 9337–9391, 2015

Evaluation of global fine-resolution precipitation products

W. Qi et al.

Title Page
Abstract
Introduction
Conclusions
References
Tables
Figures
◀I
▶I
◀
▶
Back
Close
Full Screen / Esc
Printer-friendly Version
Interactive Discussion

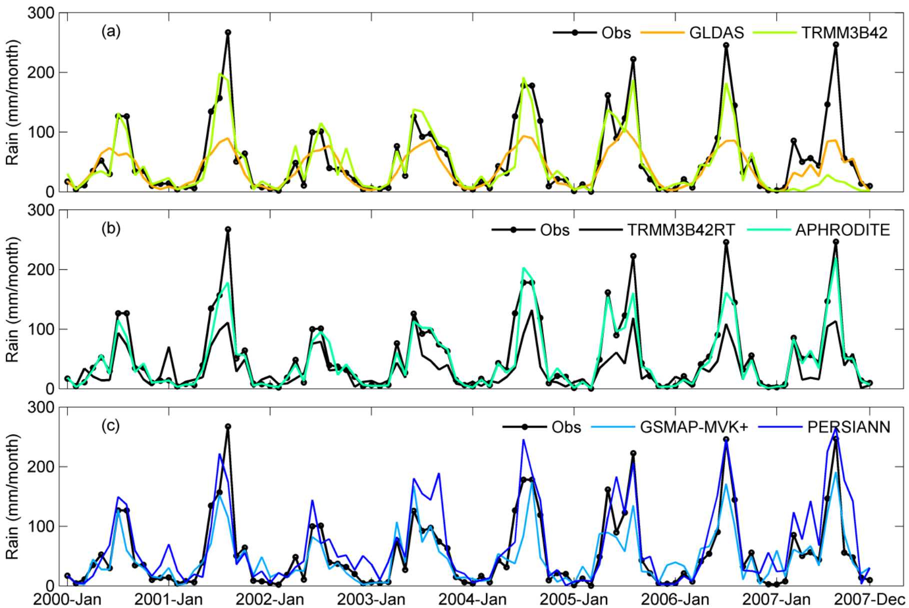


**Figure 8.** Same as Fig. 7, but in time series plots.





HESSD
12, 9337–9391, 2015

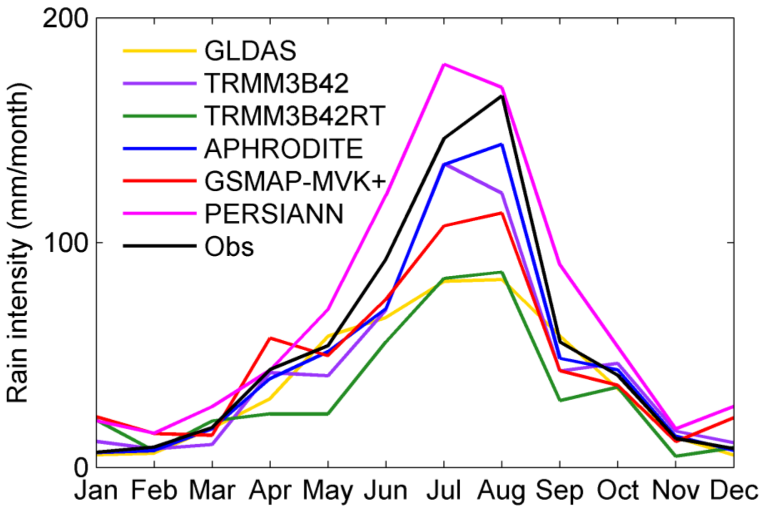


**Figure 9.** Inter-annual average monthly precipitation.

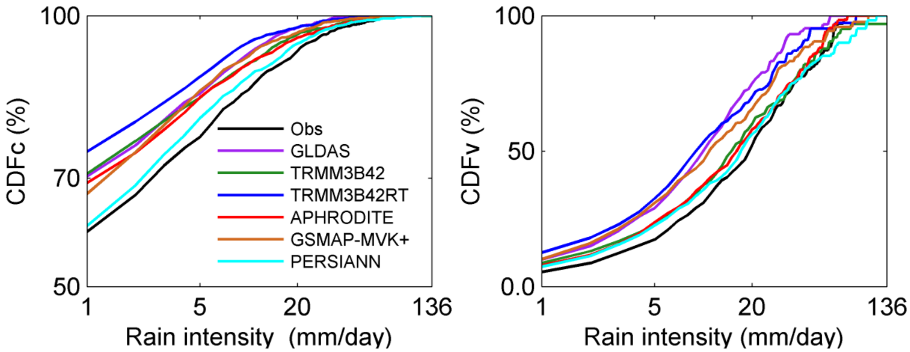


**Figure 10.** Probability distributions of the six precipitation products by occurrence (CDFc) and volume (CDFv).

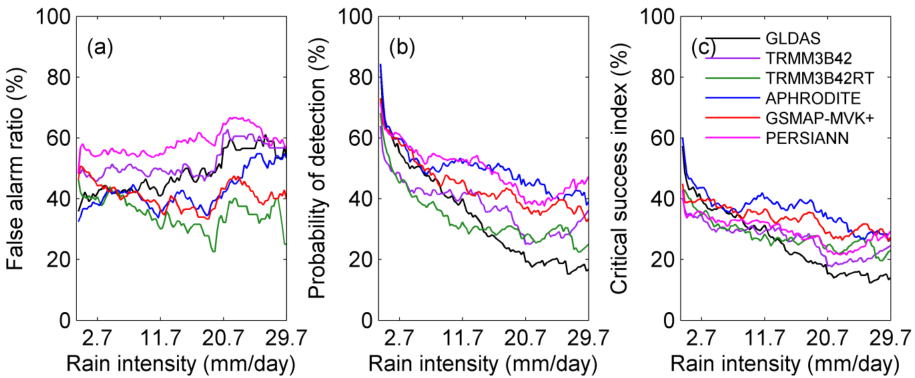


**Figure 11.** Probability of detection, false alarm ratio and critical success index for the six precipitation products.





HESSD
12, 9337–9391, 2015

Evaluation of global fine-resolution precipitation products

W. Qi et al.

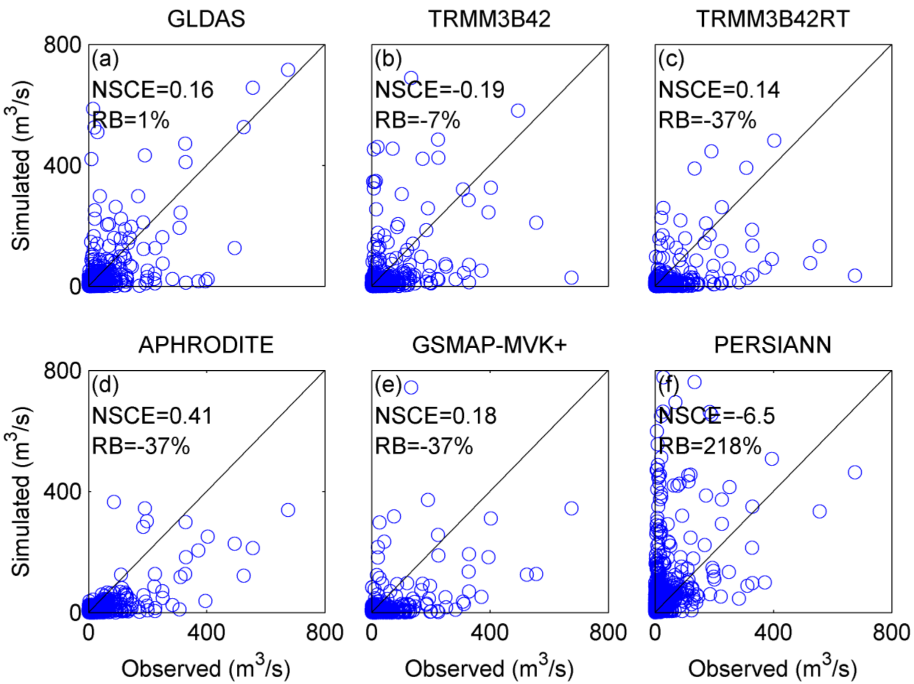


**Figure 12.** Scatterplots of simulated discharges with WEB-DHM against observations at a daily scale.





HESSD
12, 9337–9391, 2015



Title Page
Abstract | Introduction
Conclusions | References
Tables | Figures
◄◄ | ►►
◄ | ►
Back | Close
Full Screen / Esc
Printer-friendly Version
Interactive Discussion

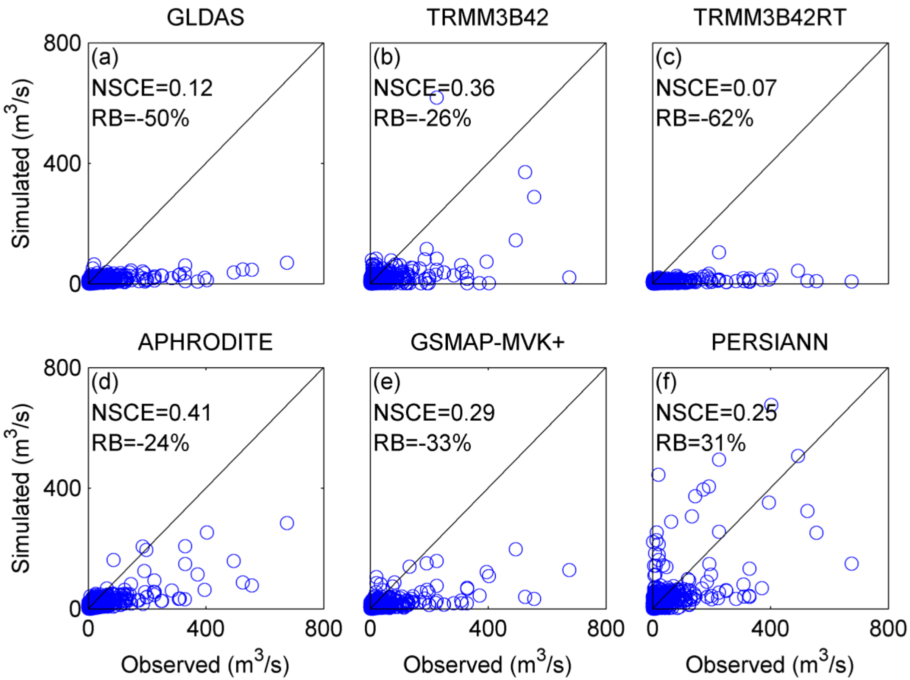


**Figure 13.** Scatterplots of simulated discharges with TOPMODEL against observations at a daily scale.

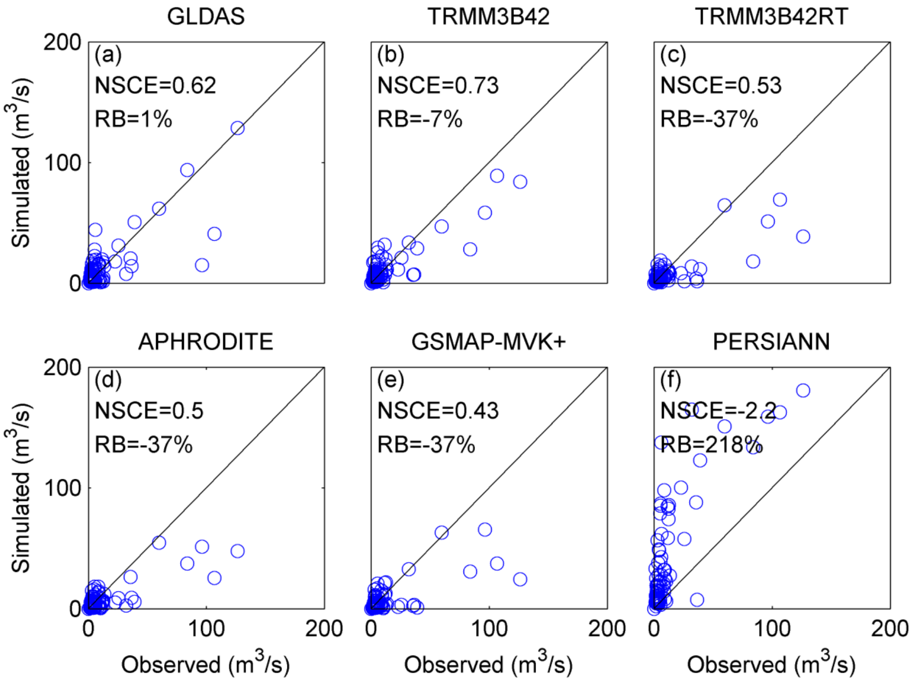


**Figure 14.** Scatterplots of simulated flow with WEB-DHM against observations at a monthly scale.





HESSD
12, 9337–9391, 2015

Evaluation of global fine-resolution precipitation products

W. Qi et al.

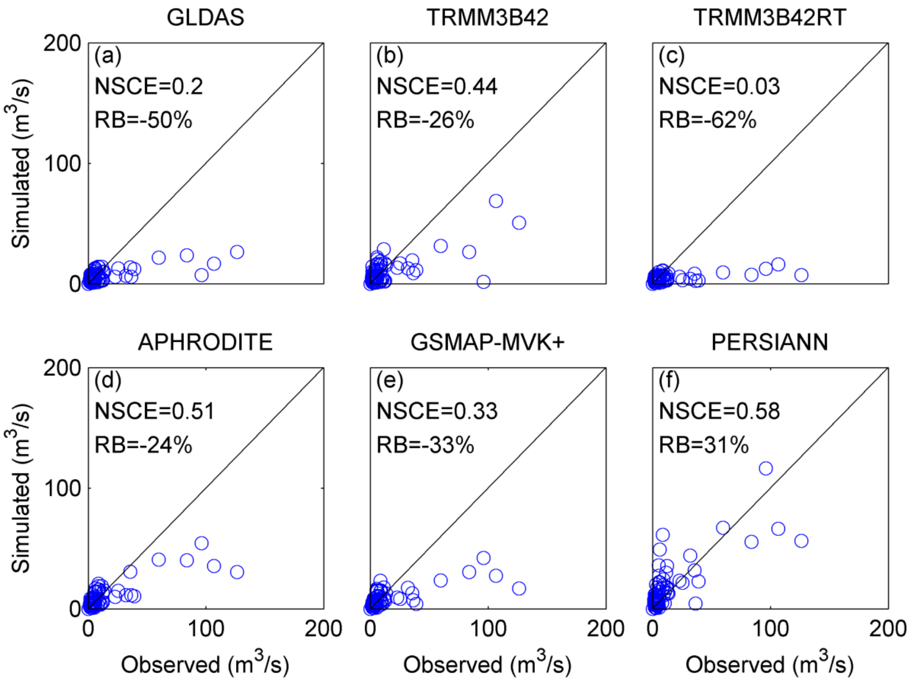


**Figure 15.** Scatterplots of simulated discharges with TOPMODEL against observations at a monthly scale.





HESSD
12, 9337–9391, 2015

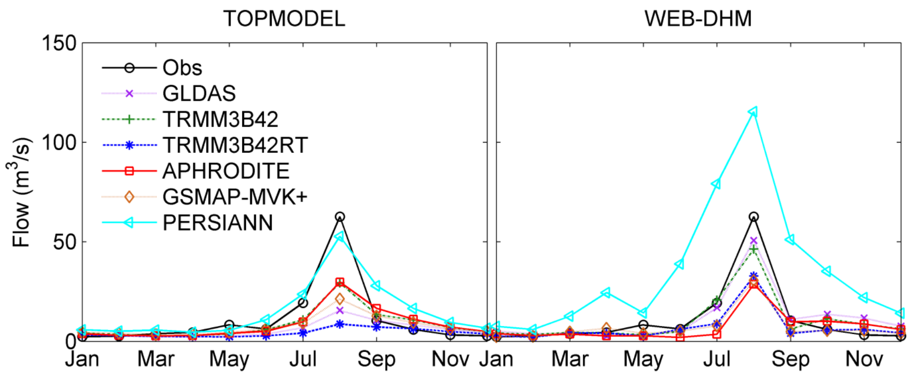


**Figure 16.** Inter-annual average monthly discharges.

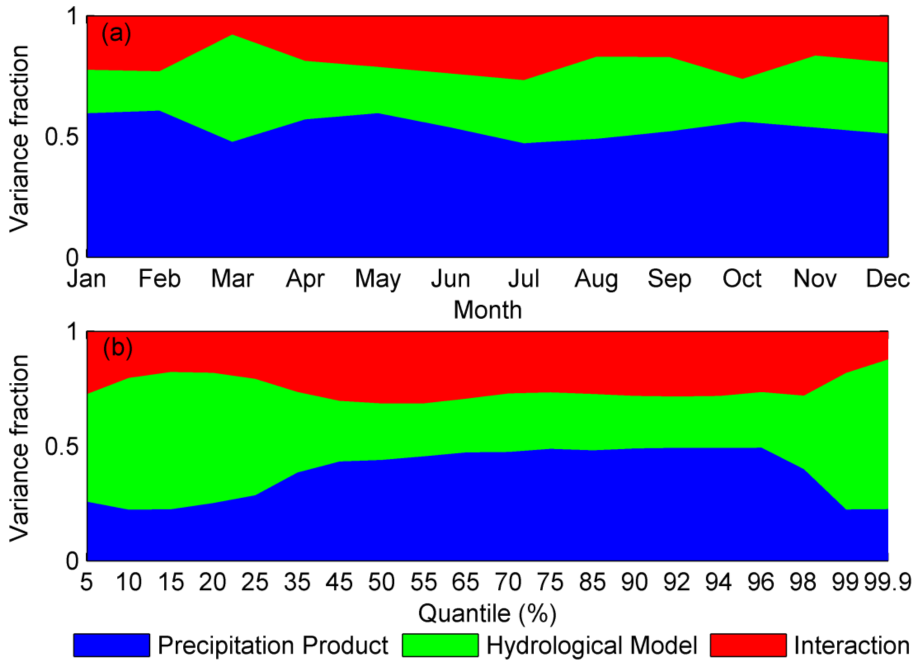


**Figure 17.** Contributions of uncertainty sources to average monthly discharges and discharge quantiles based on daily scale simulated results.





HESSD
12, 9337–9391, 2015

Evaluation of global fine-resolution precipitation products

W. Qi et al.

Title Page
Abstract
Introduction
Conclusions
References
Tables
Figures
◀I
▶I
◀
▶
Back
Close
Full Screen / Esc
Printer-friendly Version
Interactive Discussion